MASARYKOVA
UNIVERZITA

PŘÍRODOVĚDECKÁ FAKULTA

Simulace ohřevu povrchu neutronových hvězd pomocí jiskrových událostí v jejich polárních čepičkách

Diplomová práce

Bc. Tatiana Rievajová

Brno, jaro 2025

MASARYKOVA
UNIVERZITA

PŘÍRODOVĚDECKÁ FAKULTA

Simulace ohřevu povrchu neutronových hvězd pomocí jiskrových událostí v jejich polárních čepičkách

Diplomová práce

Bc. Tatiana Rievajová

Vedoucí práce: Mgr. Jan Benáček, Ph.D.

Ústav teoretické fyziky a astrofyziky

Brno, jaro 2025

MUNI
PŘÍRODOVĚDECKÁ
FAKULTA

Bibliografický záznam

Autor:	Bc. Tatiana Rievajová Přírodovědecká fakulta Masarykova univerzita Ústav teoretické fyziky a astrofyziky

Název práce:	Simulace ohřevu povrchu neutronových hvězd pomocí jiskrových událostí v jejich polárních čepičkách
Studijní program:	Fyzika
Obor:	Astrofyzika
Vedoucí práce:	Mgr. Jan Benáček, Ph.D.
Akademický rok:	2024/2025
Počet stran:	xiii + 46
Klíčová slova:	pulzar, particle-in-cell, simulace, jiskrová událost, ohřev povrchu

Bibliographic record

Author:	Bc. Tatiana Rievajová Faculty of Science Masaryk University Department of theoretical physics and astrophysics

Title of Thesis:	Simulations of neutron star surface heating by spark events in their polar caps
Degree Programme:	Physics
Field of Study:	Astrophysics
Supervisor:	Mgr. Jan Benáček, Ph.D.
Academic Year:	2024/2025
Number of Pages:	xiii + 46
Keywords:	pulsar, particle-in-cell, simulation, spark event, surface heating

Abstrakt

Pulzary jsou přírodní laboratoře pro zkoumání fyziky neutronových hvězd a poskytují cenný vhled do vlastností velmi husté hmoty, extrémně silných magnetických polí a relativistických plazmových procesů. Z různorodé populace pulzarů nabízejí zejména driftující a nulující pulzary příležitost ke studiu fyzikálních podmínek na povrchu hvězdy a v oblasti polárních čepiček. Tyto pulzary vykazují specifické chování — periodické posuny fáze pulzů a dočasná přerušení rádiového signálu — které je považováno za důsledek nelineární interakce mezi jiskrovými událostmi a ohřevem povrchu. Současné teoretické modely těchto interakcí jsou založeny především na zjednodušených analytických řešeních, což ponechává nezodpovězené otázky ohledně jejich nelineární dynamiky a pozorovatelných projevů. Cílem této práce je vyvinout plně kinetický numerický model ohřevu a ochlazování povrchu v polárních čepičkách pulzarů s využitím particle-in-cell kódu ACRONYM. Tento model bude zkoumat, jak se teplota vyvíjí v reakci na jiskrové události a jak tento zpětnovazební mechanismus ovlivňuje vznik a potlačení jisker.

Abstract

Pulsars are natural laboratories for exploration of neutron star physics, offering insights into dense matter, intense magnetic fields, and relativistic plasma processes. From the diverse pulsar population, drifting and nulling pulsars specifically provide an opportunity for studying physical conditions at the stellar surface as well as the polar cap regions. These pulsars exhibit distinct behaviors — periodic shifts in pulse phase and temporary cessation of radio emission — that are thought to result from nonlinear interaction between spark events and surface heating. Current theoretical models describing these interactions rely primarily on simplified analytical solutions, leaving open questions about the nonlinear dynamics and their observational signatures. This thesis aims to develop a fully kinetic numerical model of surface heating and cooling of pulsar polar caps, using the particle-in-cell ACRONYM code. The model will explore how temperature evolves in response to the spark cascade and how this feedback loop influences the generation and suppression of sparks.

MUNI
SCI

MASARYKOVA UNIVERZITA
PŘÍRODOVĚDECKÁ FAKULTA
KOTLÁŘSKÁ 2, 611 37 BRNO
IČ: 00216224
DIČ: CZ00216224

ZADÁNÍ DIPLOMOVÉ PRÁCE

Akademický rok: 2024/2025

Ústav:	Ústav teoretické fyziky a astrofyziky
Studentka:	Bc. Tatiana Rievajová
Program:	Fyzika
Specializace:	Astrofyzika

Ředitel *ústavu* PřF MU Vám ve smyslu Studijního a zkušebního řádu MU určuje diplomovou práci s názvem:

Název práce:	Simulace ohřevu povrchu neutronových hvězd pomocí jiskrových událostí v jejich polárních čepičkách
Název práce anglicky:	Simulations of neutron star surface heating by spark events in their polar caps
Jazyk práce:	angličtina

Oficiální zadání:

Pulsars are excellent laboratories for the physics of neutron stars and their magnetospheres because their emissions occur in the most extreme conditions in terms of tremendous star density, properties of its matter and magnetic field intensity. Two special categories of neutron stars were found that can help us to reveal the star matter's properties from observations - drifting pulsars, where the rotation phase of the radio pulse periodically shifts, and nulling pulsars, which switch between radio-emitting and radio-quite states. The physical interpretation of both pulsar categories can be related by star surface heating and cooling in regions where the emission originates, in their polar caps. Both processes are strongly nonlinear and consist of spark cascades that heat the surface and of surface radiation and plasma evaporation that can cool the surface, eventually suppressing the spark cascade for a certain time. Moreover, the current description of this interaction consists only of a analytical description of the process, opening the questions of nonlinear properties of the mechanism and the impact on the observed radiation.

The aim of the thesis is to describe the surface heating and cooling processes by a novel nonlinear numerical model that uses a recently developed particle-in-cell kinetic simulations of the pulsar polar cap. The student will study the surface temperature of the neutron star in the polar cap, its evolution, and possible impact on the spark cascades.

Plan of activities:

1. Study of the surface heating and cooling processes in the polar cap
2. Design of the implementation into the kinetic code
3. Implementation and testing of the novel approach
4. Carrying out a larger-scale simulation(s)
5. Data processing and investigation of the processes
6. Compiling of the results into the thesis

Literature:

- Gurevich, A. V., Beskin, V. S., Istomin, Ya. N., Cambridge University Press. Physics of the Pulsar Magnetosphere. (Cambridge University Press, 1993).
- Philippov, A. and Kramer, M. Pulsar Magnetospheres and Their Radiation. 65 (2022).
- Basu, R., Melikidze, G. I. and Mitra, D. Two-dimensional Configuration and Temporal Evolution of Spark Discharges in Pulsars. ApJ 936, 35 (2022).
- Mitra, D., Basu, R., Melikidze, G. I. and Arjunwadkar, M. A Single spark model for PSR J2144-3933. Monthly Notices of the Royal Astronomical Society 492, 2468–2480 (2020).

Vedoucí práce:	Mgr. Jan Benáček, Ph.D.
Datum zadání práce:	27. 11. 2023
V Brně dne:	6. 5. 2025

Bc. Tatiana Rievajová, 27. 11. 2023
Mgr. Jan Benáček, Ph.D., 1. 12. 2023
Mgr. Dušan Hemzal, Ph.D., 13. 12. 2023

Acknowledgements

First and foremost, I would like to thank my amazing supervisor Mgr. Jan Benáček, Ph.D., for his enormous patience and ever-present guidance. I am thankful for all the opportunities you gave me to learn as much as possible. I appreciate all that you taught me, and I cannot imagine a better supervisor (although I know you can imagine a better student).

I would also like to thank my family, who supported me during my studies. And a special thank you to my beloved sister, for her moral support, constant hugs, and pictures of cats.

Declaration

Hereby I declare that this paper is my original authorial work, which I have worked out on my own. All sources, references, and literature used or excerpted during elaboration of this work are properly cited and listed in complete reference to the due source. I acknowledge the use of OpenAI's ChatGPT as a writing assistant for help in structuring and polishing certain sections of this work.

Brno 6. 5. 2025 Bc. Tatiana Rievajová

Contents

Introduction

Pulsars are rapidly rotating and highly magnetized remnants of massive stars. They are one of the enigmas of astrophysics research. Since their discovery, pulsars have been considered as natural laboratories for exploring matter under extreme conditions, the behavior of strong magnetic fields, and the physics of relativistic plasmas. At the heart of pulsar theory lies the concept of a magnetosphere filled with electron–positron plasma, where electromagnetic fields and plasma currents interact in complex ways to produce observable radiation. The plasma in these environments is typically collisionless, meaning that collective electromagnetic effects and instabilities dominate over particle collisions.

A main challenge in pulsar astrophysics is understanding the origin and properties of their coherent radio emission, widely believed to be generated in the polar cap regions through pair cascades and plasma instabilities. These processes are governed by the local kinetic plasma phenomena as well as the global structure of the magnetosphere. Advances in computational astrophysics, particularly the development of large-scale particle-in-cell (PIC) simulations, have allowed researchers to model these kinetic processes from first principles, capturing the nonlinear evolution of plasma, particle acceleration, and electromagnetic wave generation with unprecedented accuracy. Such simulations have become essential for elucidating the physics of pulsar magnetospheres and for linking theoretical models to observations.

This thesis is structured as follows. The first two chapters provide an overview of the fundamental properties of pulsars, the theoretical model of their magnetospheres with the pair creation mechanism, emission processes, and drifting and nulling pulsars are introduced. The following chapter describes the PIC simulation method and its application to pulsars, detailing the numerical techniques and physical models employed. The final chapter presents the results of kinetic simulations of pair cascades and electromagnetic wave generation in the polar cap, analyzing how local plasma conditions shape the spark cascade.

1 Pulsars

The journey to a neutron star starts at the final stages of a massive star's life. When the core of a massive star depletes all of its energy sources, all the way to iron, and the outer layers of the star are ejected by a supernova explosion, there is one last stable stage in the stellar evolution.

A supernova explosion is an event where the star explodes and the outer layers are ejected into space around the star. After the explosion, all that is left of the massive star is its core, the so-called supernova remnant. The supernova remnant does not always have to be there. Sometimes, there is nothing left. There are several types of supernovae, but only the core-collapse supernovae can create a neutron star (Lyne & Graham-Smith, 2012).

After the massive star, with an initial mass between 8 and 20 $M_\odot$, burns out hydrogen and helium in the core, heavier elements start to burn in the shells around. The nuclear reactions stop at iron because the process of iron burning is an exothermic reaction and it cannot create the necessary energy to fuel the star. In the newly formed iron core with mass above 1.4 $M_\odot$ and temperature around 10^9 K, energetic electrons and protons form neutrons and neutrinos

$$p + e^- \rightarrow n + \nu_e, \tag{1.1}$$

and high-energy photons can interact with iron, fragmenting into several helium nuclei. The core loses in this manner a great amount of energy $E \sim 10^{46}$ J, and the inner pressure that contributed to the core's stability disappears, leading to the core's collapse. The amount of released energy is large enough to explain the observed kinetic energy of the ejected material in the supernovae (Longair, 2011).

1.1 Discovery of neutron stars

Shortly after the discovery of a neutron, the possibility of a star created mainly by neutrons was discussed. Walter Baade and Fritz Zwicky in 1934 came with a theoretical model of such a star, which was two decades before the neutron stars were first observed. They linked the creation of neutron stars with supernovae, but predicted very low luminosities for observations. The idea of a link between supernova remnants and neutron stars was grounded in the understanding of stellar evolution and the Chandrasekhar limit. According to this limit, a white dwarf exceeding 1.4 $M_\odot$ will collapse under its own gravity, forming a neutron star or a black hole, depending on the exact mass and other factors (Lyne & Graham-Smith, 2012).

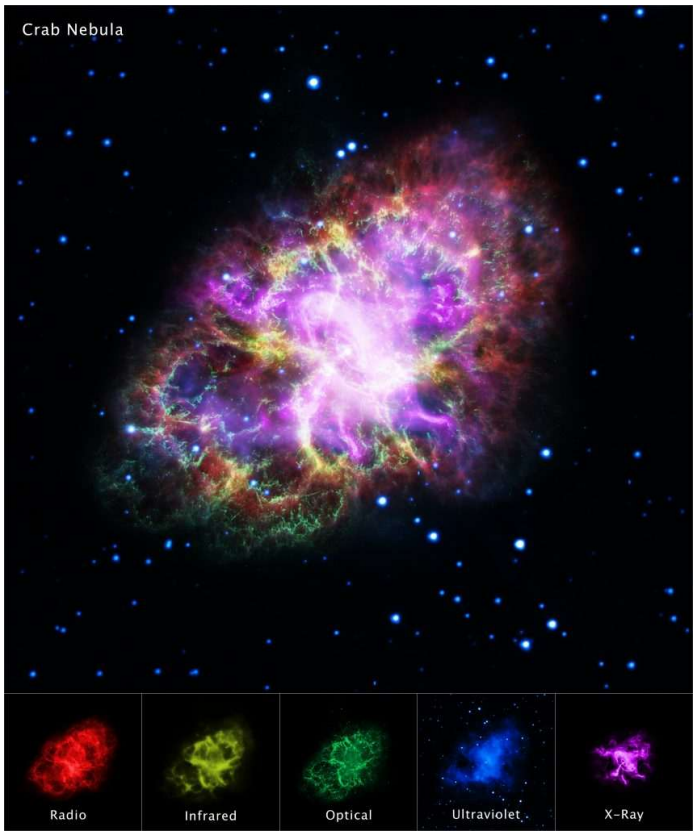

Figure 1.1: Image of the Crab Nebula created by combining data from telescopes spanning nearly the entire width of the electromagnetic spectrum, from the radio waves to the high-energy waves. Credit: *G. Dubner (IAFE, CONICET-University of Buenos Aires) et al.; NRAO/AUI/NSF; A. Loll et al.; T. Temim et al.; F. Seward et al.; Chandra/CXC; Spitzer/JPL-Caltech; XMM-Newton/ESA; and Hubble/STScI.*

The theoretical models developed in the following years provided more details about the structure and properties of neutron stars. These models were working with principles from nuclear physics and the general theory of relativity to derive the equation of state of neutron-dense matter. One of the first proposals came from Oppenheimer and Volkoff in 1939. The equation of state is crucial for determining the internal structure, stability, and sets a limit to the maximum mass of a neutron star.

The first observational evidence for neutron stars came when L. Hewish 1968 together with his student Jocelyn Bell discovered a periodical radio signal at lower frequencies. After a closer look, they found that the signal was composed of a series of short pulses, coming from the source PSR 1919+21. It was the first observation not only of a neutron star but also of a pulsar. The observed pulses had very stable, short period and were polarized, which

was soon explained by a model of fast rotating, highly magnetized neutron star (Pacini, 1967).

Observational proof of the origin of a neutron star was the detection of the pulsar in the Crab Nebula and in the Vela supernova remnant. They were both young pulsars, their age corresponding with the supernova explosion as well as the age of the material around them, left after the explosion. Moreover, the very short rotational period of the Crab pulsar ($\sim$ 33 ms) excluded other possible origins of pulsars and definitely related pulsars to neutron stars (Longair, 2011).

The most recent discovery connected to the neutron stars was the detection of the gravitational wave event GW170817, which confirmed that the merger of two neutron stars produces gravitational waves. For gravitational wave detection is also interesting the use of pulsar timing array, which involves several different pulsars in our galaxy, but also outside of it (Abbott et al., 2017).

Ongoing research, both observational and theoretical, promises to further unravel the mysteries of these fascinating objects.

1.2 Classification of neutron stars

As was indicated above, there are several different types of neutron stars. The main characteristics are the same, such as their composition, fast rotation, small radius, and strong magnetic field. A typical neutron star can be considered to have a period of several seconds, a magnetic field in the order of 10^{12} G, a radius around 10 km, and a mass up to 1.4 $M_\odot$. The star can be observed in X-rays, in some cases because of its surface temperature in the order of 10^6 K.

1.2.1 Pulsars

The main characteristic of pulsars is the observed radio emission from these sources. When the rotational axis of the neutron star is not aligned with the magnetic axis, we can observe pulses of radio emission emitted along the magnetic axis. Due to the misalignment of the axes, the rotation of the star causes the observed regular pulses of radiation, creating the lighthouse effect. The pulses come to the observer with a period corresponding to the rotation of the star. The origin and exact process of creation of the coherent radio emission are still open questions (Lorimer & Kramer, 2004).

The striking regularity of pulses allows for measuring the short periods very accurately. The measurements are so precise that a small steady slowdown of the pulse period is detected. This slowdown rate $\dot{P}$ is one of the defining parameters of pulsars (Longair, 2011).

1.2.2 Magnetars

A special group of neutron stars are magnetars. Their main peculiarity is the extremely strong magnetic field enhanced by dynamo effects up to the 10^{15} G. Within such an extreme field, several quantum-mechanical effects take place and cannot be neglected. When the massive star collapses and creates a supernova explosion, the decisive factor whether a classical neutron star or a magnetar is created is the speed of the rotation. With fast enough rotation, a dynamo is produced, which can amplify the magnetic field (Rosswog & Brüggen, 2007).

1.2.3 Millisecond pulsars

After the discovery of pulsars and their very fast rotation, nobody even thought there could be any stars with even faster rotation. It lasted until 1982, when the first millisecond pulsar was found in a very strong radio source, similar to the Crab pulsar. After a detailed analysis of the data, the period of the radio pulses turned out to be 1.56 ms. Because of the need for difficult computations involved in the analysis, the systematic search for similar objects came only after the advance in computer power in 1990s. The millisecond pulsars are a part of a binary system and can be found very rarely as an isolated star (Longair, 2011).

1.2.4 Binary pulsars

From the beginning, all neutron stars were considered isolated stars, in theoretical models and also from observations, since no periodic Doppler shift was measured in the pulse period. The first signal indicating a binary system came in 1975 from pulsar PSR B1913+16. The distance of the binary was found to be comparable to the dimension of our Sun. It was unusually close, considering the orbital period was determined as only a couple of hours long. This system was found to be composed of one neutron star and one pulsar (Longair, 2011).

Binary pulsars are an excellent laboratory for testing the general theory of relativity, as well as measuring very precisely the masses of neutron stars. Part of the test for general relativity is a direct observation of the shortening orbital period, which can be caused by a release of energy in the form of gravitational waves. Today, several different binary pulsars are known. In some binaries, both stars are pulsars, or there are others where one of the components is a black hole.

1.3 Interesting properties

Neutron stars exhibit extreme physical properties, placing them at the outermost limits of known matter behavior. As a result, they represent a unique space laboratory for testing all different kinds of theories from different fields. One of the extreme properties is the density of the matter inside the star, which can reach as high as 10^{17} kg m^{-3}, producing degenerate neutron gas. Combined with the fast rotation and a very strong magnetic field, these conditions cannot yet be recreated to be studied on Earth (Longair, 2011). Some of the key physical properties and processes associated with pulsars are magnetic braking, $P\dot{P}$ diagram, internal structure, and their magnetospheres.

One of the interesting properties is the slight increase in rotational period as the rotational energy E_{rot} is transformed into electromagnetic radiation. This process, called magnetic braking, takes place when the magnetic axis is misaligned with the rotation axis. As the pulsar rotates, the magnetic dipole radiates electromagnetic pulses powered by the rotational energy. For calculating the energy loss rate, it is necessary to know the spin-down rate and the period of the pulsar

$$\frac{\mathrm{d}E_{\text{rot}}}{\mathrm{d}t} = -4\pi^2 I \frac{\dot{P}}{P^3}, \tag{1.2}$$

where I is the moment of inertia, and P is the period of the pulsar. From this, the age of the pulsar can be estimated, with the assumption of constant magnetic braking, as

$$\tau = \frac{P}{2\dot{P}}. \tag{1.3}$$

From this equation, a typical age of an average pulsar is in the range of $10^5 - 10^8$ years (Lorimer & Kramer, 2004). Apart from the age, the strength of the magnetic field can be likewise calculated from equation 1.2, and it directly depends on the values of P and $\dot{P}$. For this reason, a $P\dot{P}$ diagram for pulsars is something like the Hertzsprung-Russell diagram (HRD) for stars. Similar to HRD, the $P\dot{P}$ diagram reveals the diversity of pulsar populations and their evolutionary paths. As the pulsars get older, they slow down and move down in the diagram. Magnetars with extremely strong magnetic fields have very long periods as opposed to the millisecond pulsars in the left corner of the diagram, clearly showing the effect of magnetic braking (Longair, 2011).

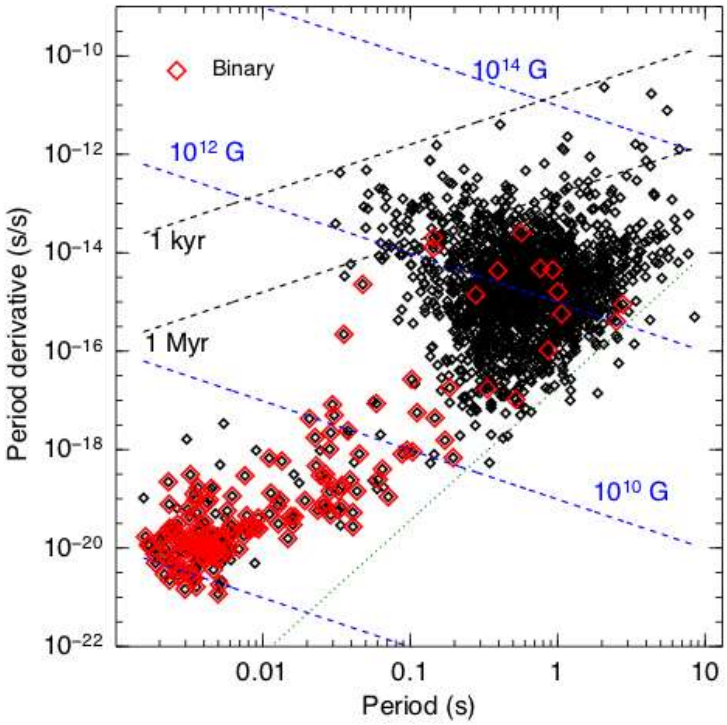

Figure 1.2: The $P\dot{P}$ diagram. Newly created pulsars after supernova explosion are located in the upper left corner. During their evolution, they slowly move down and to the right. Almost all pulsars with a short period (millisecond pulsars) are part of a binary system (denoted in red). Credit: *https://neutronstars.utk.edu/code/nstar-plot/ppdot.html#p-pdot-diagram*.

Based on the theoretical models and calculations, the idea is that there is an outer crust and an interior composed of degenerate neutron gas. In the outer crust can be found different ions, mainly iron nuclei. As the density increases towards the center, the atoms are pushed closer together. The electrons start to combine with protons into neutrons, creating new isotopes of heavier elements like Krypton (Longair, 2011). Gradually, the neutron-rich nuclei dissolve into a neutron fluid. The inner core reaches values bordering on the density of nuclear matter, and its exact composition is still a mystery. There is a handful of theories, from exotic matter to mesons. The internal structure of the neutron star is closely related to the equation of state. However, it is not yet clear how exactly the equation of state looks like. From mass and radius measurements, some constraints exist, as well as from observed irregularities in the pulses (Lorimer & Kramer, 2004).

1.4 Pulsar magnetosphere

The magnetosphere of a pulsar is a highly structured and dynamic region dominated by the star's strong magnetic field and filled with plasma. The magnetosphere plays a crucial role in the pulsar's observable characteristics, particularly its emission mechanisms and pulse profiles.

The configuration of the magnetic field is typically modeled as a rotating, inclined dipole. The plasma in the magnetosphere is compelled to co-rotate with the pulsar but the co-rotation is only sustainable up to a certain distance known as the light cylinder radius. At this imaginary cylindrical boundary, the velocity of co-rotating plasma reaches the speed of light c. The light cylinder also divides the magnetic field lines into closed and open. Closed field lines are anchored to the star at both ends, and they are filled with dense plasma. Open field lines, which extend beyond the light cylinder radius, allow particles to escape into the interstellar medium (Lyne & Graham-Smith, 2012).

The radius of the light cylinder, $R_{\rm LC}$, is approximately determined by the pulsar's angular velocity Ω, or equivalently, its rotational period P, and can be expressed as (Hessels et al., 2006)

$$R_{\rm LC} = \frac{c}{\Omega} = \frac{cP}{2\pi}. \tag{1.4}$$

The simplest theoretical model assumes the dipole magnetic field is aligned with the rotational axis. This configuration was first described in the work by Goldreich and Julian (1969). In their model, the magnetic field is frozen into the star, and its rotation induces local electric fields. These fields can be partially screened by the moving charged particles when the magnetosphere is filled with enough plasma. A balance is achieved between the induced electric field and a static electric field $\mathbf{E}$, resulting in a force-free magnetosphere given by:

$$\mathbf{E} + (\mathbf{v} \times \mathbf{B}) = \mathbf{E} + \frac{1}{c}\,(\Omega \times \mathbf{r}) \times \mathbf{B} = 0, \tag{1.5}$$

where $\mathbf{v}$ is the velocity of the charged particles, $\mathbf{r}$ is the position vector, and $\mathbf{B}$ is the magnetic field. This force-free model primarily describes regions with dense plasma populations, such as those within closed magnetic field lines.

The Goldreich–Julian model also describes the magnetospheric plasma near the star's surface. It predicts that the induced local electric field is strong enough to pull charged particles from the stellar surface. This field then accelerates these primary particles along magnetic field lines, which may lead to pair production cascades that populate the magnetosphere with electrons and positrons. The co-rotation of the created plasma helps to screen the local electric field parallel to the magnetic field, except in specific acceleration regions (Lyne & Graham-Smith, 2012).

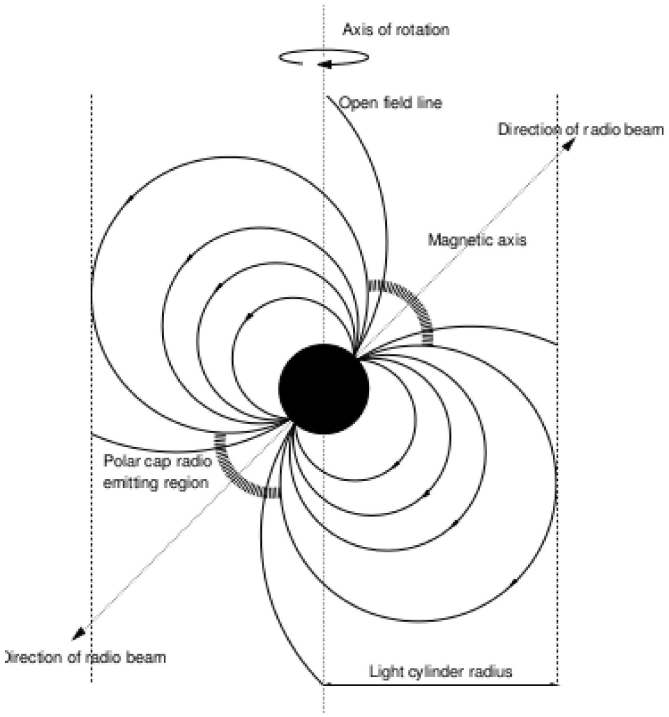

Figure 1.3: Model of the pulsar magnetosphere with the non-aligned magnetic axis. Credit: *https://www.researchgate.net/figure/The-lighthouse-model-of-the-pulsar-magnetosphere_fig*.

2 Observations and observational properties

Ever since the discovery in 1967, people have been trying to relate the theoretical models of neutron stars to their observations. For example, observations revealed that some pulsars, apart from radio waves, emit X-rays and gamma rays, indicating that neutron stars can also be sources of high-energy radiation. These different emissions provided a crucial insight into the theoretical models of both the surface and magnetospheric physical processes around the pulsar.

Beyond the characteristic periodic emission associated with their rotation, pulsars often exhibit complex single-pulse phenomena such as subpulse drifting and pulse nulling, which are connected with the underlying emission mechanisms in the magnetosphere (Basu & Mitra, 2018; Wen et al., 2016).

Radio waves are the most commonly detected form of pulsar radiation. They are believed to originate near the magnetic poles in regions called polar caps, where charged particles, accelerated along magnetic field lines, can emit coherent radiation.

In addition to radio waves, some pulsars emit thermal radiation observable in the X-ray part of the spectrum. This emission is generally blackbody-like and originates from the hot surface of the neutron star, which can potentially retain thermal energy from its formation in a supernova explosion. The surface temperatures are typically around 10^6 K, and observations of thermal emission can be used to determine fundamental stellar parameters such as their radius (Rengarajan, 1973).

Pulsars also exhibit significant non-thermal high-energy emission in the X-ray and gamma-rays. One of them is, for example, the synchrotron radiation, resulting from relativistic electrons spiraling around magnetic field lines (Harding, 2001).

2.1 Emission processes

A key concept for pulsar radio emission is the polar cap, which is defined by the open magnetic field lines that extend outward from the magnetic poles of the neutron star. The processes in the polar cap are critical because they are the source of particles that escape along the open field lines into the magnetosphere and beyond. This region also features large potential differences that can accelerate particles to extreme energies, depending on the pulsar's rotation period and magnetic field strength (Harding & Muslimov, 1998).

The acceleration of particles in the polar cap results in a variety of radiation processes. The inner acceleration gap, situated just above the polar

cap, is one of the proposed origins of strong electric fields. These fields accelerate electrons (or positrons) along magnetic field lines. As these particles follow curved paths along the magnetic field, they emit curvature radiation, a candidate for the origin of pulsar radio waves. To explain the high brightness temperature observed, the charged particles must radiate in phase, significantly boosting the intensity of the emitted signal (Melikidze et al., 2000).

For the coherent emission, the generation of pair cascades is important. In these cascades, high-energy photons, produced by synchro–curvature radiation, interact with the intense magnetic fields to produce electron-positron pairs. These pairs can then themselves radiate and create further cascades, amplifying the particle density in the emission regions. Such activity can create a particle outflow that can be associated with individual pulses or subpulse structures seen in some pulsar observations.

While radio emission arises close to the star, just above the polar caps, in a region influenced by coherent plasma processes, high-energy emission originates farther out, where particles continue to be accelerated and radiate incoherently (Benáček et al., submitted in March 2025; Crinquand et al., 2021).

2.1.1 Polar cap and pair cascades

The size of the polar cap is determined by the geometry of the pulsar's magnetic field and rotation, typically amounting to a fraction of the star's radius. Due to rotationally induced charge separation and the inability of the magnetosphere to supply enough charge locally, strong electric fields can develop above the polar cap. These fields can sustain a potential drop of the order of 10^{12} volts, sufficient to accelerate electrons to ultra-relativistic energies. These particles can then emit high-energy photons (Longair, 2011).

In the presence of a strong magnetic field ($\mathbf{B} \gtrsim 10^{12}$ G), these photons can interact with the field to produce electron–positron pairs. This leads to a pair cascade, where each generation of particles emits photons, sustaining the process. The result is a dense, relativistic pair plasma streaming outward along the open field lines (Cruz et al., 2021; Timokhin & Harding, 2019). For these particles to emit coherently, they must be arranged in spatially compact bunches with a phase coherence. The emitted power is scaled as the square of the number of participating particles (Mitra et al., 2015).

The exact nature of these coherent processes remains an open question, but several theoretical frameworks suggest that plasma instabilities, such as two-stream instabilities in relativistic plasma, can give rise to such emission. These instabilities may also lead to maser amplification or produce soliton structures that emit coherently. The radiation is often interpreted as coherent

curvature radiation from plasma bunches moving along magnetic field lines. Observational support for coherence includes the highly polarized nature of pulsar radio emission and its rapid time variability on microsecond scales (Basu et al., 2025).

The classical vacuum gap model (Ruderman & Sutherland, 1975) describes the inner acceleration region of pulsars as a near-vacuum zone above the magnetic polar cap. However, this model assumes an idealized dipolar magnetic field and does not align well with X-ray observations showing small, hot polar caps and strong, localized surface fields.

The partially screened gap (PSG) model describes the inner acceleration region with incorporated thermal ion emission regulated by surface temperature, which is maintained near a critical value by returning particles from cascades. For example, Szary et al. (2015) identified two distinct PSG modes, depending on the dominant gamma photon production mechanism.

In the PSG-off mode, negligible ion emission allows high acceleration, and curvature radiation dominates. Primary particles reach Lorentz factors, produce gamma rays at higher altitudes, and the returning pairs eventually heat the surface, but the delayed feedback keeps the gap mostly unscreened.

In contrast, the PSG-on mode involves inverse Compton scattering, enabled by partial ion screening. Particle acceleration is limited, but gamma rays are produced close to the surface, ensuring continuous heating and stable plasma generation.

These two regimes explain phenomena like pulse nulling and mode-changing in pulsars. The PSG model, grounded in surface physics and non-dipolar magnetic fields, offers a unified framework for pulsar emission behavior.

2.1.2 High-energy emission

Incoherent processes such as cyclotron, synchrotron, and curvature radiation dominate in the high-energy regimes of pulsar emission, particularly in X-rays and gamma rays.

Cyclotron radiation arises from non-relativistic charged particles spiraling around magnetic field lines. The emission is at the fundamental Larmor frequency and its harmonics, and is typically weak unless occurring in dense or highly magnetized plasma. Though fundamental in principle, cyclotron radiation plays a relatively minor role in pulsar magnetospheres (Labaj et al., 2024; Lyne & Graham-Smith, 2012).

More important is the synchrotron radiation, which is produced by relativistic electrons spiraling in magnetic fields with non-zero pitch angles. In this case, the emitted power is beamed along the particle's velocity vector and can exhibit strong polarization characteristics. The synchrotron spectrum

peaks at a critical frequency dependent on both the Lorentz factor of the particle and the magnetic field strength. Self-absorption can occur at lower frequencies, leading to a turnover in the observed spectrum, particularly in compact regions of high electron density (Kelner et al., 2015).

Closely related is the curvature radiation, which is particularly relevant in the context of pulsar radio emission. Unlike synchrotron radiation, curvature radiation does not require a pitch angle, as it arises from relativistic particles constrained to follow curved magnetic field lines. In the tightly curved field geometry of a pulsar's inner magnetosphere, curvature radiation becomes highly efficient. The power radiated and the critical frequency depend sensitively on the particle energy and the radius of curvature of the field lines, making this process especially suitable for explaining the broadband, high-energy emission from pulsars (Gil et al., 2004).

Inverse Compton scattering also contributes to the high-energy emission from pulsars, particularly in gamma rays. The low-energy photons can gain energy through collisions with high-energy electrons. Photons originating from the neutron star surface or the synchrotron background may be scattered by high-energy particles in the outer magnetosphere, leading to non-thermal gamma-ray emission. This process is supported by observations of broad spectral energy distributions, such as those from the Crab pulsar, which span from the ultraviolet to very high-energy gamma rays. These observations have been effectively modeled using cyclotron-self-Compton scenarios (Lyutikov, 2013; Lyutikov et al., 2012).

In addition to non-thermal emission, pulsars can also emit significant thermal radiation, primarily in the soft X-ray and far ultraviolet. The thermal spectrum typically resembles a blackbody, although deviations may occur due to atmospheric effects and anisotropies. In young pulsars, such as the Crab and Vela, this emission is detectable as a distinct component in their composite X-ray spectra. In older pulsars, surface cooling results in a reduced thermal flux, but localized heating, especially near the polar caps, may sustain detectable levels of soft thermal X-rays (Borghese & Zelati, 2025).

Thermal radiation from the polar cap is particularly relevant in the context of particle acceleration models. As charged particles return to the surface along magnetic field lines, they deposit energy, heating the polar cap to temperatures higher than the rest of the star. This backstreaming heating can create localized hotspots, which serve as sources for thermal photon processes like inverse Compton scattering (Gil et al., 2003).

Therefore, thermal emission plays a dual role: as an observable indicator of neutron star surface temperature and as a source of photon field for high-energy scattering processes. It complements the non-thermal emission mechanisms and provides insight into the thermal and magnetic structure of neutron stars.

2.2 Drifting pulsars

Drifting pulsars are a type of neutron star whose radio emissions exhibit periodic modulation, in the form of subpulses that drift across the pulse window. The drifting of subpulses was first observed in the 1970s and is commonly explained by the model proposed by Ruderman and Sutherland (1975).

According to this model, in the pulsar's polar cap there are multiple sparks regions with intense electric fields. These sparks rotate around the magnetic axis due to the combined effects of the neutron star's rotation and the electric field. The motion of these sparks leads to the observed drifting of subpulses across the pulse profile.

Subpulses are visible as distinct intensity peaks within the main radio pulse, and can systematically move across pulse longitude over successive rotations of the pulsar. This behavior was first identified by Drake and Craft (1968). In drifting pulsars, the subpulses do not occur randomly but exhibit an organized pattern that can be described by two characteristic parameters: the longitudinal separation between adjacent subpulses and the vertical separation between drift bands across successive pulses. Together, these parameters define the drift rate and pattern observed. Detailed studies have shown that subpulse drifting is a widespread phenomenon, with surveys by Weltevrede et al. (2006) finding that a significant fraction of pulsars, possibly more than half, show some form of drifting behavior when observed with adequate sensitivity and time resolution.

The drift direction is typically uniform across the pulse profile. However, certain pulsars exhibit a more complex behavior known as "bi-drifting," where subpulses in different components of the pulse profile drift in opposite directions. This phenomenon challenges the simplicity of the model and suggests a more intricate structure within the pulsar's magnetosphere (Weltevrede, 2016).

The study of drifting pulsars relies heavily on high-resolution time-domain observations. Instruments such as the Five-hundred-meter Aperture Spherical Radio Telescope (FAST) and the Green Bank Telescope (GBT) are used to obtain detailed pulse profiles and fluctuation spectra. These observations allow for the identification and analysis of subpulse drifting behavior across different frequencies, providing insights into the frequency dependence of the drifting phenomenon (Basu et al., 2016).

Furthermore, the study of subpulse drifting provides information about the geometry of the pulsar's magnetosphere and the structure of its emission regions. By analyzing the drift patterns and their frequency dependence, properties such as the inclination angle between the magnetic and rotational

axes, the geometry of the polar cap, and the distribution of sparks within the magnetosphere can be found (McSweeney et al., 2019).

2.3 Nulling pulsars

Pulse nulling is the abrupt, often unpredictable, absence of observable radio emission from a pulsar, lasting for one or more rotation periods before the emission resumes. First discovered by Backer (1970), pulse nulling has since been found in a wide range of pulsars, though its occurrence and characteristics vary significantly from one source to another. In nulling pulsars, the absence of detectable emission is simultaneous across a range of frequencies, strongly suggesting that the effect is intrinsic to the pulsar's magnetosphere rather than being caused by propagation effects such as scintillation or absorption in the interstellar medium (Gajjar et al., 2014).

The nulling fraction (NF), defined as the percentage of time a pulsar is observed in the null state, is a primary quantitative descriptor of this behavior. Studies have reported NFs ranging from fractions of a percent to over 90% (Ritchings, 1976; Wang et al., 2007), with some extreme cases, termed intermittent pulsars, showing on-off emission states lasting thousands of rotations.

Despite decades of studies, the physical mechanism underlying pulse nulling remains uncertain. Several theoretical explanations have been proposed, including changes in the conditions for pair production near the magnetic poles, temporary cessation of coherent radio emission processes, and large-scale magnetospheric reconfigurations. Some models suggest that nulling may represent a transitional evolutionary phase as pulsars get older and approach the point where the potential drop across the polar gap becomes insufficient to sustain the particle cascades necessary for radio emission. However, statistical analyses by Konar and Deka (2019) have shown no simple correlation between nulling behavior and basic pulsar parameters such as characteristic age, period, or derivative of the period, suggesting a more complicated origin. In addition, they have important implications for pulsar population statistics and the detectability of pulsars in surveys. The nulling can reduce the observed pulse energy, making pulsars harder to detect and potentially biasing population estimates. Understanding the nature and cause of the nulling is therefore of both theoretical and observational importance.

While many nulling pulsars exhibit apparently random occurrences of emission cessation, some show evidence for quasiperiodic nulling, where the nulls repeat at approximately regular intervals. This behavior, first identified systematically by Herfindal and Rankin (2007, 2009), indicates the presence of a periodic process within the pulsar magnetosphere. Quasiperiodic nulling

suggests that the conditions leading to the cessation and resumption of emission may involve cyclic changes in the magnetospheric configuration, plasma supply, or coherent radiation processes. The existence of an internal timescale governing these transitions opens a new path for studying the dynamics of the pulsar magnetosphere beyond simple on-off behavior (Xu et al., 2024).

In some pulsars, quasiperiodic nulling occurs alongside subpulse drifting, although the two phenomena typically exhibit different periodicity. For example, the periodicity associated with subpulse drifting is usually much shorter than the periodicity associated with quasiperiodic nulling. Studies by Basu et al. (2016, 2017) have shown that while drifting periodicity appears weakly anticorrelated with the pulsar's spin-down energy loss rate, quasiperiodic nulling shows no such clear dependence or with any other pulsar parameter. This indicates that although both phenomena involve periodic modulation of the observed emission, they likely originate from different physical mechanisms.

3 Plasma simulations

Plasma simulations and numerical modeling play a crucial role in understanding the complex behavior of pulsar magnetospheres. These environments are governed by extreme electromagnetic fields and relativistic plasma, and their accurate modeling requires sophisticated computational techniques.

One of the most widely used methods for simulating pulsar magnetospheres is the Particle-in-Cell (PIC) technique. PIC simulations are particularly valuable because they enable a self-consistent treatment of both the electromagnetic fields and the kinematics of individual plasma particles (Cruz et al., 2024; Manthei et al., 2021). For example, A. A. Philippov et al. (2015) conducted three-dimensional PIC simulations of aligned pulsar magnetospheres. Their work demonstrated how these systems can transition from charge-separated electrosphere states to more force-free-like configurations when sufficient pair plasma is supplied to the system.

In addition to pure PIC methods, hybrid approaches have been developed to address the significant computational challenges involved in simulating pulsars. These challenges arise because of the enormous differences in scale between particle motion and the global magnetospheric structure. To overcome this, Soudais et al. (2024) have proposed a hybrid numerical scheme that combines ideal force-free and PIC methods. Their hybrid model was applied to simulate the magnetosphere of a weakly magnetized millisecond pulsar. Remarkably, they were able to reproduce key observational features, including strong synchrotron radiation consistent with gamma-ray data from telescopes like Fermi-LAT.

Another important aspect of pulsar magnetospheric modeling is the method by which plasma is injected into the system. Different plasma injection models can lead to different magnetospheric structures. Recent studies, using simulation tools such as the OSIRIS framework, have explored a variety of injection methods. For example, Cruz et al. (2024) included volume-based, surface-based, and pair-production-based injection schemes. The results indicate that, depending on the plasma supply rate, the magnetosphere can either approximate a force-free solution or revert to an electrosphere-like state.

Finally, plasma simulations are essential for connecting the theoretical models and observational data. In particular, they help to explain the origins of radio, X-ray, and gamma-ray emissions detected from pulsars.

3.1 Particle-in-cell simulations

Particle-in-cell (PIC) simulations are a computational framework designed to model kinetic plasma dynamics by self-consistently describing how charged particles interact with electromagnetic fields. In these simulations, charged particles are represented as discrete macro-particles, each carrying a weighted charge-to-mass ratio describing a certain number of real particles, and their trajectories are tracked through the phase space. To minimize numerical noise, these macro-particles are assigned a shape function, which smooths their contributions to the grid. The motion of each particle is determined by the relativistic Lorentz force, written in the CGS units as

$$\frac{\mathrm{d}\mathbf{p}}{\mathrm{d}t} = q\left(\mathbf{E} + \frac{\mathbf{v}\times\mathbf{B}}{c}\right), \tag{3.1}$$

where $\mathbf{p}$, q, and $\mathbf{v}$ denote momentum, charge, and velocity, respectively. This equation is typically integrated using a leapfrog scheme, which staggers particle positions and velocities in time to maintain numerical stability and to increase the order of precision.

Electromagnetic fields are solved on an Eulerian grid using discretized forms of Maxwell's equations. The electric field $\mathbf{E}$ and magnetic field $\mathbf{B}$ are updated through Faraday's and Ampère's laws, written also in CGS,

$$\nabla\times\mathbf{E} = -\frac{1}{c}\frac{\partial\mathbf{B}}{\partial t}, \tag{3.2}$$

$$\nabla\times\mathbf{B} = \frac{4\pi}{c}\mathbf{J} + \frac{1}{c}\frac{\partial\mathbf{E}}{\partial t}, \tag{3.3}$$

with the current density $\mathbf{J}$ derived from the collective motion of particles. Charge conservation is enforced through specialized current deposition techniques, such as Esirkepov's method (Esirkepov, 1999), which ensures that the continuity equation

$$\nabla\cdot\mathbf{J} = -\frac{\partial\rho}{\partial t}, \tag{3.4}$$

holds to the machine precision, preventing field artifacts, and increasing energy conservation.

The PIC simulation cycle involves several steps that are iteratively repeated. First, the charge and current densities of particles are deposited onto the grid according to their positions and velocities. Next, Maxwell's equations are solved on the grid to update the electromagnetic field components. These updated fields are then interpolated back to the positions of the particles, enabling the calculation of the Lorentz force on each particle. Finally, the velocities and positions of the particles are updated using the equations of motion. This sequence ensures a fully self-consistent treatment of particle-field interactions that is capable of capturing a wide range of kinetic phenomena.

PIC methods are particularly advantageous in astrophysical contexts where relativistic plasma and strong electromagnetic fields dominate, such as in the magnetospheres of pulsars. In these environments, analytical approaches are often insufficient due to the nonlinearity of the equations and the dynamic nature of the plasma.

In pulsar magnetospheric modeling, PIC simulations are used to investigate various aspects of plasma behavior. One significant application is the modeling of pair production and pair cascade, which are crucial for maintaining a stable magnetospheric structure.

Additionally, PIC simulations have been employed to investigate the development of plasma instabilities, such as the streaming instabilities, which may play a role in generating coherent radio emission from pulsars. These instabilities arise because of velocity differences between different particle populations and can lead to the growth of plasma waves that emit observable radiation (Manthei et al., 2021).

Despite their strengths, PIC simulations also face several challenges. One of the limitations is their high computational cost. Because of the need to resolve microscale phenomena like the Debye length and plasma frequency, which can conflict with the vast spatial and temporal scales of astrophysical systems.

In summary, PIC simulations constitute a powerful and versatile approach for investigating the kinetic plasma physics of pulsar magnetospheres. They have enabled significant progress in understanding plasma injection, magnetospheric structure, particle acceleration, radiation processes, and wave-particle interactions. As computational capabilities continue to improve, PIC methods are expected to play an increasingly central role in the study of the electrodynamics of pulsars and related astrophysical systems.

3.2 ACRONYM code

In this work, the ACRONYM code (Another Code for pushing Relativistic Objects, Now with Yee lattice and Macro particles) was used for the simulations. It is a highly flexible, explicit PIC code designed for modeling plasma processes in one, two, or three spatial dimensions. It supports an arbitrary number of charged particle species, with particle motion calculated using the relativistically adapted Boris push algorithm. That ensures accurate treatment of particle dynamics even at relativistic velocities, which is essential for application ("Acronym PIC code", n.d.; Kilian et al., 2012).

ACRONYM is capable of simulating both electrostatic and electromagnetic plasma models, offering a range of field solvers and particle pushers, and their shape functions to accommodate various physical scenarios. The interpolation between field quantities (defined on the grid) and particle

quantities is handled through a selection of shape functions, allowing users to tailor the code's numerical properties to their specific needs.

A notable feature of ACRONYM is its scalability and parallelization: the code is MPI-parallelized and has been successfully deployed on computational platforms ranging from single-board computers to some of the world's largest supercomputers. This makes it suitable for both small-scale exploratory studies and large-scale, high-resolution simulations.

The code has been applied to a wide range of plasma physics problems, including magnetic reconnection, collisionless shocks, and plasma emission processes. During this thesis, the updated version of the code was used, with mainly the addition of the magnetospheric current described in our work Benáček et al. (2024) where I also contributed.

3.3 Numerical implementation details

In this thesis, we are interested in whether the star's surface heated by sparks can release enough matter from the star's surface to suppress or otherwise change the radio wave emission. To simulate and study the effects of surface heating and thermionic emission, it is necessary to implement the heating and cooling equations into the numerical code ACRONYM. With high temperature, too much plasma is released from the surface because of thermionic emission. The pair cascade or spark event then does not occur because the electric fields accelerating the particles in the spark are screened out by the dense plasma. After a certain time, the plasma outflows, and the sparks occur again. This indicates there must be a quasi-equilibrium of the plasma released from the star, depending on the surface temperature.

Several nonlinear processes take place and cause temperature changes. Plasma released during the spark cascade heats the surface, which leads to surface X-ray blackbody radiation and plasma also evaporates from the surface. The evaporation and X-ray thermal radiation cool down the surface, and contrary to what is needed for the pulsar emission, the spark stops. This scenario could explain the mechanism behind drifting and nulling pulsars.

The main equations and parameters crucial for these simulations are described in Gil et al. (2003). In this paper, the depth of heat deposition and surface layer properties are discussed in the context of polar cap heating due to backflowing particles in the partially screened gap (PSG) model. In the PSG model, the polar cap surface of a neutron star is subject to intense heating due to the bombardment by relativistic particles. These particles, electrons or positrons, are accelerated in the inner acceleration gap region of the polar cap and flow back toward the surface during spark event. Understanding how this energy is deposited and dissipated is crucial for modeling the thermal regulation and dynamics of the gap.

The kinetic energy of the incoming particles is deposited within an extremely thin layer at the stellar surface. According to Gil et al. 2003, this depth is estimated to be, depending on the strength of the magnetic field, between

$$L \sim 0.3 - 3\,\mathrm{mm}. \tag{3.5}$$

Such shallow penetration is due to the high density of the surface material, which efficiently absorbs the energy of the incoming relativistic particles. Because of this limited penetration depth, the thermal energy is concentrated in a very narrow region, which has important consequences for the cooling and thermal timescales of the surface.

The density in this uppermost layer of the neutron star crust is typically in the range of

$$\rho_s \sim 10^3 - 10^4\,\mathrm{g/cm^3}. \tag{3.6}$$

This value is consistent with the properties of a solid crust composed predominantly of iron nuclei, as expected for neutron star surface. The combination of high density and small depth means the thermal inertia of this layer is low, enabling it to respond rapidly to changes in heating.

Because of its limited thickness and high thermal conductivity, the heated surface layer cools down very quickly. The characteristic cooling timescale, or e-folding time, is estimated to be on the order of

$$\tau_{\mathrm{cool}} \sim 1 - 100\,\mu\mathrm{s}. \tag{3.7}$$

However, only a small drop in surface temperature, just a few percent, may be sufficient to significantly affect the rate of thermionic emission. Therefore, effective thermal regulation can occur on even shorter timescales, comparable to or faster than the typical gap emptying time, which is in the order of 10 ns.

The surface temperature T_s of the polar cap is determined by a balance between radiative cooling and heating from particle bombardment. This energy balance can be expressed as

$$\sigma T_s^4 = \eta\, \gamma_{\mathrm{acc}}\, m_e c^3 n_{\mathrm{GJ}}, \tag{3.8}$$

where σ is the Stefan-Boltzmann constant, η is the shielding factor describing the fractional unscreened potential drop, γ_{acc} is the Lorentz factor of accelerated particles, m_e is the electron mass, c is the speed of light, and n_{GJ} is the Goldreich-Julian number density.

As the surface heats up, the rate of thermionic emission of ions or electrons increases, which leads to more effective screening of the electric field (i.e., a lower value of η). This reduces the potential drop in the gap and thus the energy of incoming particles, which in turn reduces the heating. On the other hand, if the surface temperature drops, the emission weakens, the electric

field grows stronger, and the heating intensifies. This dynamic forms a tightly linked thermodynamic feedback loop.

As a result, the surface temperature should be stabilized just below the critical value needed for full thermionic emission, either T_i for ions or T_e for electrons. Typically, the temperature difference between the actual surface temperature and the critical value is of the order of

$$\Delta T = T_i - T_s \sim 10^4\,\mathrm{K},$$

meaning that even small thermal fluctuations could trigger or suppress spark activity. This sensitive balance is fundamental to the quasi-periodic nature of sparking in the PSG model and supports a self-regulated discharge mechanism that is consistent with the observed subpulse drifting behavior in many pulsars.

4 Simulations and results

Since the global kinetic simulations of pulsar magnetospheres lack the resolution necessary to capture the small-scale physics of a polar cap, instead, I focus only on a small local region that co-rotates with the neutron star, where the plasma scales can be resolved. In this local frame, I want to study the effects of heating and cooling of the star's surface and its influence on cascades and plasma bunches.

I utilize a fourth-order M24 field solver proposed by Greenwood et al. (2004), which is well-suited for high-accuracy electromagnetic field calculations. To mitigate numerical Cherenkov radiation, which is a common artifact in relativistic PIC simulations, I use a low-pass filter introduced by Friedman (1990), applying a filter coefficient of $\theta = 0.1$. For the current deposition, I apply the charge-conserving scheme developed by Esirkepov (2001), with a higher-order "piecewise cubic shape" (PCS) function of macro-particles. This combination ensures accurate charge conservation and smoother particle-weighting profiles. The particle dynamics are computed using a modified version of the Vay et al. (2011) particle pusher, adapted to include the gyromotion approximation described by A. Philippov et al. (2020). This approximation assumes that particles rapidly lose perpendicular kinetic energy on timescales shorter than one timestep. As a result, only the component of the electric field parallel to the local magnetic field is used in advancing particle motion.

The quantum-electrodynamic effects for pair creation are approximated using a simplified threshold-based model. When the Lorentz factor of an accelerated particle crosses a threshold value γ_{th}, a new pair is created, and 10 % of the primary particle's energy is equally divided between the new two particles. (Similar approximations are done and explained in my bachelor's thesis Rievajová (2023).)

All simulations in this work are performed using the 2D3V (two spatial dimensions, three velocity components) configuration of the ACRONYM code. The computational domain is a rectangular spatial grid, with absorbing boundary conditions along the x and y axes and infinitely long along the z axis.

4.1 Co-authored papers and their relevance

I contributed to a couple of scientific papers, and my contribution to the Benáček et al. (2024) involved a new additional way of saving data during simulation. This paper investigates the generation and propagation of electromagnetic waves in the polar cap regions of the magnetosphere, focus-

ing on the mechanisms responsible for coherent radio emission in pulsars. Two-dimensional, relativistic PIC simulations were employed, and incorporated quantum-electrodynamic pair cascades with the assumption of charge-limited flow from the neutron star surface. The paper explores three inclination angles of the magnetic dipole — $0°$, $45°$, and $90°$ — to understand how the inclination and the associated magnetospheric current profiles influence the pair cascade behavior and Poynting flux transport.

The key conclusion is that the cascade properties are significantly influenced by the magnetospheric current profiles within the polar cap. Specifically, high-intensity Poynting flux transport channels form along magnetic field lines where magnetospheric currents approach zero and the plasma is unable to sustain these currents.

The focus is on plasma dynamics and radio emission, but the pair cascade also depends on the surface heating mechanism, which needs to be more closely studied.

For more detailed analysis and a faster way of saving data, I added an option to save o 1D array from the 2D simulation grid. The same method is used for saving the surface temperature array in my simulations. Additionally, the simulation setup in this paper was used as a starting point for my simulations in this thesis. As the pair creation process and the magnetosphere of the pulsar were already implemented into the ACRONYM, all that was left to add were the heating and cooling processes.

The second paper Benáček et al. (submitted in March 2025) presents the first three-dimensional PIC simulations that investigate the polarization properties of coherent radio waves escaping from the polar caps of pulsars. The focus is on a pulsar with a magnetic inclination angle of $60°$, with again incorporated quantum-electrodynamic pair cascades and charge-limited flow from the neutron star surface in the numerical model. The aim is to clarify the initial polarization characteristics of pulsar radio emission, which are crucial for understanding radiative transfer through the magnetosphere and for interpreting observed polarization signatures.

The simulations reveal that the escaping radio emission from the polar cap can reproduce a wide range of observed pulsar properties, including the radio power, spectral shape, pulse profiles, and polarization curves. The paper demonstrates that pair discharges near the surface of the pulsar polar cap are responsible for the generation and initial polarization of pulsar radio emission, and that these processes determine many of the key observed properties. However, the main focus of the paper is on the generation and polarization of coherent radio emission, not on modeling the thermal evolution or cooling of the neutron star surface. The connection to surface heating is an important consequence of the pair cascade, but is not explored in detail within the simulations or results of this particular paper.

4.2 Thermal processes in the code

For the surface heating by back-streaming particles, the following equations were implemented. The kinetic energy of the particle, absorbed at the surface, is equal to the heat energy absorbed by the surface. The change in temperature is then calculated as

$$\Delta T = \frac{E_{\mathrm{kin}}}{C L \, \Delta x^2}, \tag{4.1}$$

where L is the depth of heat deposition in cm, Δx is a grid cell size also in cm, and C is the specific heat per unit volume, defined in Gil et al. (2003) as

$$C = 4.4 \times 10^{12} \rho_6 \left(1 + 0.024 \rho_6^{-2/3} T_6\right) \ \mathrm{erg/K/cm^3}, \tag{4.2}$$

where $\rho_6 = \rho_{\mathrm{s}}/10^6$ is the surface density, and $T_6 = T_{\mathrm{s}}/10^6$ is the surface temperature. The kinetic energy of the particle is calculated simply as

$$E_{\mathrm{kin}} = (\gamma - 1) m c^2, \tag{4.3}$$

where γ is the Lorentz factor of the particle, m is its mass, and c is the speed of light. To avoid steep spikes in temperature between neighboring grid cells representing the surface, the energy is distributed in several grids using the same PCS function as is used for macro-particles.

For the cooling of the surface, two different mechanisms were implemented. First is the thermal blackbody radiation. The radiative energy is calculated as

$$E_{\mathrm{rad}} = \sigma \, T_{\mathrm{s}}^4 \, \Delta x^2 \, \Delta t, \tag{4.4}$$

where σ is the Stefan-Boltzmann constant in CGS units, and Δt is the simulation timestep in seconds. The temperature change is then calculated the same as Equation 4.1, but instead of E_{kin}, the E_{rad} is used.

The second cooling mechanism is the heat transport. For calculating the effect of this cooling mechanism, we used a simplified approach. First, the cooling timescale described in 3.3 is calculated as

$$\tau_{\mathrm{cool}} = \frac{L^2 \, C}{\kappa}, \tag{4.5}$$

where κ is the thermal conductivity of the surface. With this cooling timescale, we can calculate how much the surface cools down in one simulation timestep

$$\Delta T = \frac{T_{\mathrm{s}} - T_{\mathrm{s,i}}}{\tau_{\mathrm{cool}}} \, \Delta t, \tag{4.6}$$

where $T_{\mathrm{s,i}}$ is the initial surface temperature.

An additional condition needed to be implemented when the cooling mechanisms are so effective that the surface temperature is cooled below the initial surface temperature $T_{\mathrm{s}} < T_{\mathrm{s,i}}$. In this case, the temperature was set to the initial surface temperature value.

4.3 Surface temperature evolution

Following the completion of implementing the heating and cooling, I performed a set of testing simulations to investigate the evolution of surface temperature with different initial values. I conducted the simulations using a simple setup in order to isolate and analyze whether there is any thermal response of the system. The result is shown in Figure 4.1, where the evolution of temperature became identical for all cases very quickly after the first cascade events. This shows that the effects of heating by backstreaming particles from cascades do not depend on the initial temperature. It also confirms the effectiveness of cooling, as the temperature seems to stabilize around a value $T_s = 2 \times 10^7$ K.

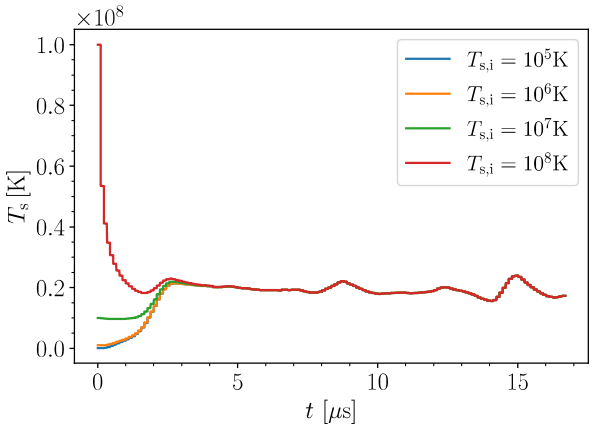

Figure 4.1: Time evolution of the surface temperature for different initial values of $T_{s,i}$.

Using the same simulation setup, an additional correlation in the time evolution of temperature is presented in Figure 4.2. The x axis represents position across the stellar surface while the y axis represents time. The first spark occurs around $\omega_p t = 500$, which coincides clearly with a sharp increase in surface temperature. This can be explained as one particle species (positron or electron) created in the cascade is accelerated towards the surface, where it is absorbed, and its kinetic energy is transformed into heat. The plasma created during the first cascade effectively screens the accelerating electric field and prevents further cascade generation, until the plasma flows away from the region. During this time, the surface continues to cool down, but is no longer heated, causing a decrease in temperature. For the remaining time of the simulation, each subsequent increase in the temperature aligns with the occurrence of a new cascade, indicating a strong temporal correlation between localized heating and discharege activity.

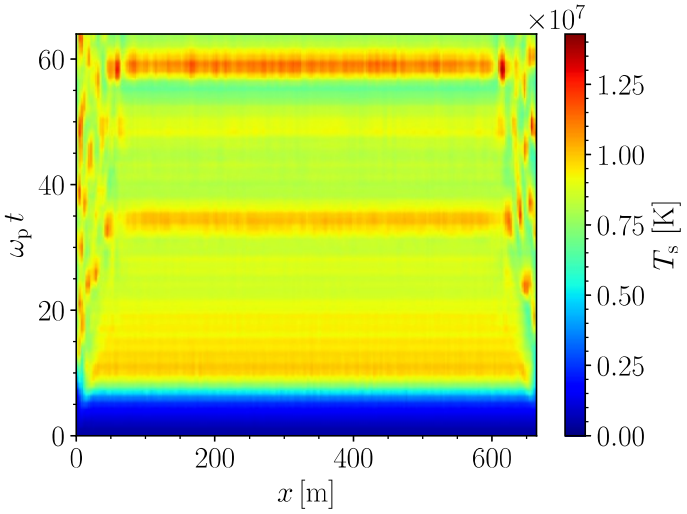

Figure 4.2: Time evolution of the surface temperature along the star surface.

4.4 Colling effects

Two distinct cooling mechanisms are considered: the blackbody radiation and thermal heat transport. Figure 4.3 presents the results of two similar simulation setups, comparing two scenarios – one in which only blackbody radiation is active, and another where only heat transport is enabled. The results indicate that blackbody radiation serves as a significantly more effective cooling mechanism in this system. When only heat transport is included, the temperature increases steadily over time, and no clear correlation with cascades is observed.

In contrast, simulations involving blackbody radiation exhibit distinct temperature rises that align with the cascade activity. This behavior is further illustrated in Figure 4.3 (right panel), where both cooling mechanisms are active, reinforcing the dominant role of radiative cooling in regulating surface temperature.

4.5 Small-scale simulations

I performed two small-scale simulations to obtain the difference that the thermal effects have on the cascades. The initial parameters of the simulations are in Table 4.1. The simulation y-axis is always parallel to B_{dipole} and the grid size is $\Delta = 333.5$ cm. The real size of the domain is then 667m $\times$ 1334m. The star surface is located around $50\Delta \approx 167$m from the bottom simulation boundary.

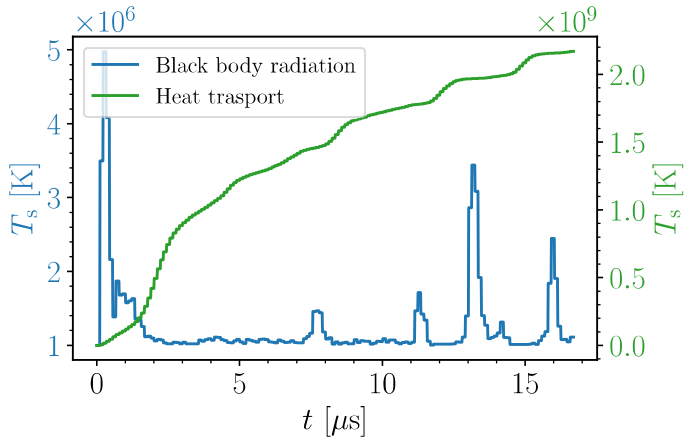

Figure 4.3: Time evolution of the surface temperature with only blackbody radiation cooling mechanism (blue), and with only a heat transport cooling mechanism (green).

The initial electric field is set to zero in the simulation, and the magnetic field **B** is given only by the dipole magnetic field. When the simulation starts, all particles have the Goldreich-Julian charge density and thermal velocity distribution function.

The first simulation was run without thermal effects, while the second included both heating and cooling processes. Shortly after the start of the simulations, the first cascade occurs at approximately the same time in both cases. However, a slight difference in the total particle density is already detectable.

This difference became more pronounced in subsequent cascades. As the simulations evolved, the differences between the two cases, in terms of total particle density and the parallel component of the electric field, became increasingly apparent, as is shown in Figure 4.4.

Although the number and frequency of cascades remain similar, the simulation with thermal effects consistently exhibits higher particle densities during cascades. Furthermore, the structure of the particle bunches generated in the heated case showed distinct variations, indicating that thermal feedback can influence both the local plasma conditions and the morphology of the bunches.

At the end of the simulations shown in Figure 4.5, the clear difference in the positron and electron densities shows that with the thermal processes, the particles are more localized above the surface, depending on the temperature of the surface. Whereas, when the heating is turned off, the density is more uniform across the x axis.

By the end of the simulations, there is a clear difference in the spatial distribution of positron and electron densities. In the case with thermal processes enabled, particles are more strongly localized above a certain part of the stellar surface. In contrast, when heating is disabled, the particle density appear more uniform along the x axis, indicating the absence of temperature-driven local effects. This suggests that thermal feedback plays a significant role in shaping the structure of bunches near the surface.

Table 4.1: Parameters for small-scale simulations.

Parameter	Value
Star period	0.25 s
Star mass $M_\star$	$1.5\,\mathrm{M}_\odot$
Star radius $R_\star$	10 km
Dipole inclination i	0°
Dipole field B_{dipol}	10^{12} G
Dimensions	$200\Delta \times 400\Delta \times 1\Delta$
Timestep	$3000\Delta t$
Grid cell size Δ	333.5 cm
Simulation timestep Δt	5.56 ns
Plasma frequency ω_p	$4 \times 10^6\,\mathrm{s}^{-1}$
$\omega_\mathrm{p}\Delta t$	0.022
Friedman filter θ	0.1
Particle decay threshold γ_th	2×10^7
Initial surface temperature T_s	10^6 K
Critical ion temperature T_ion	1.01×10^6 K
Depth of heat deposition L	0.003 cm
Surface density ρ_s	$4.45 \times 10^3\,\mathrm{g/cm}^3$
Thermal conductivity of the surface κ	1.6×10^{11} erg/cm/s/K

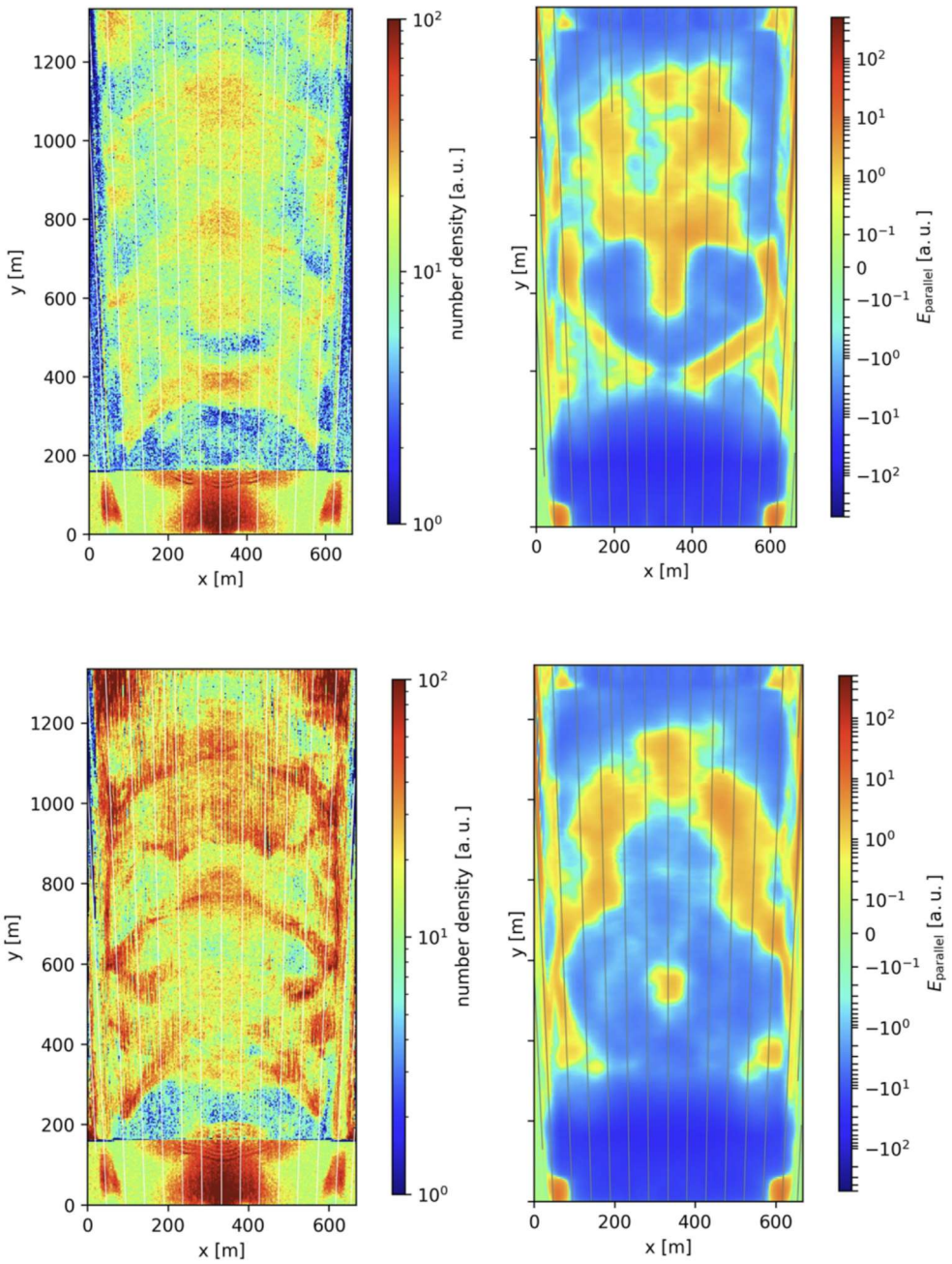

Figure 4.4: Comparison of total number density (left) and parallel component of the electric field (right) in two different simulations at time $\omega_p t = 22$. One without the thermal effects (top row) and one with the thermal effects (bottom row). The gray lines represent the magnetic field lines.

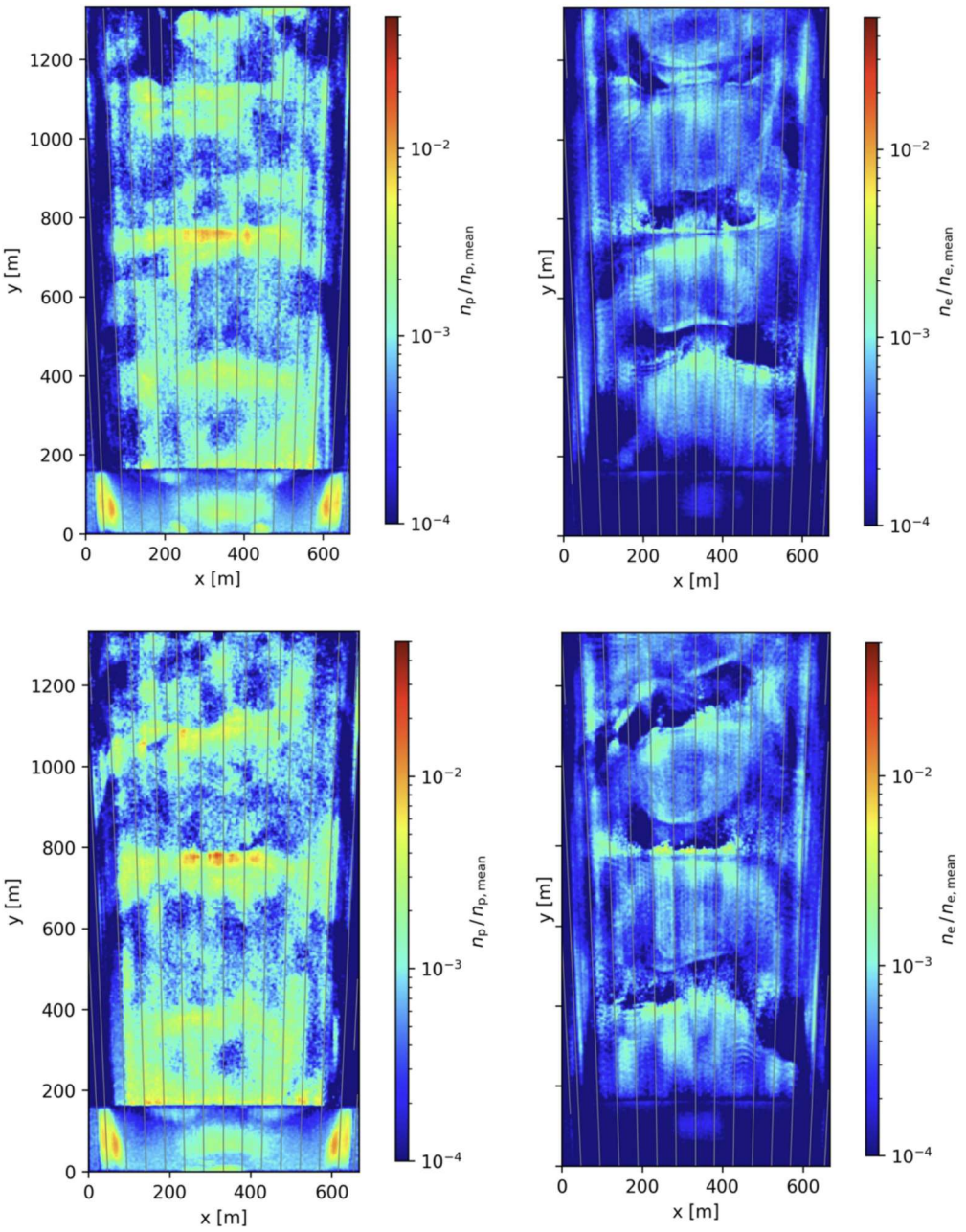

Figure 4.5: Comparison of charge density of positrons (left) and charge density of electrons at the end of the simulations. One simulation is without the thermal effects (top row) and one with the thermal effects (bottom row). The gray lines represent the magnetic field lines.

4.6 Different initial parameters

Another objective of this thesis is to assess whether, and to what extent, the thermal effects depend on variations in initial surface parameters, specifically surface density and the depth of heat deposition. Within the scientific community, there is an ongoing debate where one viewpoint emphasizes that these parameters are critical, arguing that the thermal response and associated mechanisms are highly sensitive to their values. In contrast, others contend that these surface parameters have a limited impact on the overall dynamics and on the mechanisms believed to drive the observed radio emission.

To investigate this, we performed two additional simulations using the same baseline parameters outlined in Table 4.1. In the second simulation, the surface density was increased to $\rho_s = 4.45 \times 10^4 \mathrm{g/cm}^3$. Despite this change, the simulation outcomes remained largely consistent, with no significant differences observed during the early and mid phases. Only after several cascades did a small difference in total particle density become apparent, as illustrated in Figure 4.6.

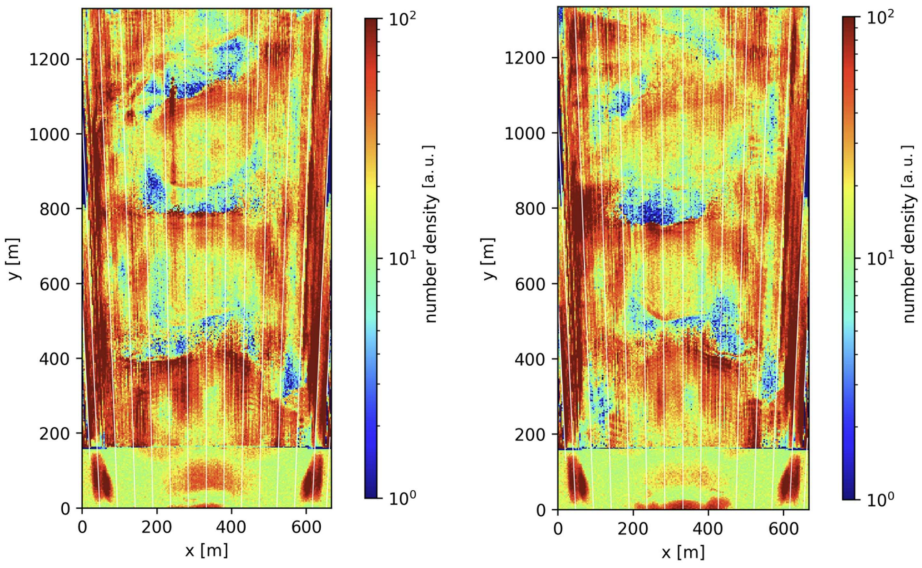

Figure 4.6: Comparison of the total number density at the end of the simulation. They have different values of surface density, on the left is $\rho_s = 4.45 \times 10^3 \mathrm{g/cm}^3$ and on the right $\rho_s = 4.45 \times 10^4 \mathrm{g/cm}^3$. The gray lines represent the magnetic field lines.

Similarly, when the depth of heat deposition was adjusted to $L = 3 \times 10^{-4}$ cm, the overall behavior of the system remained stable. Again, only minor

deviations in particle density were observed near the end of the simulation, as shown in Figure 4.7.

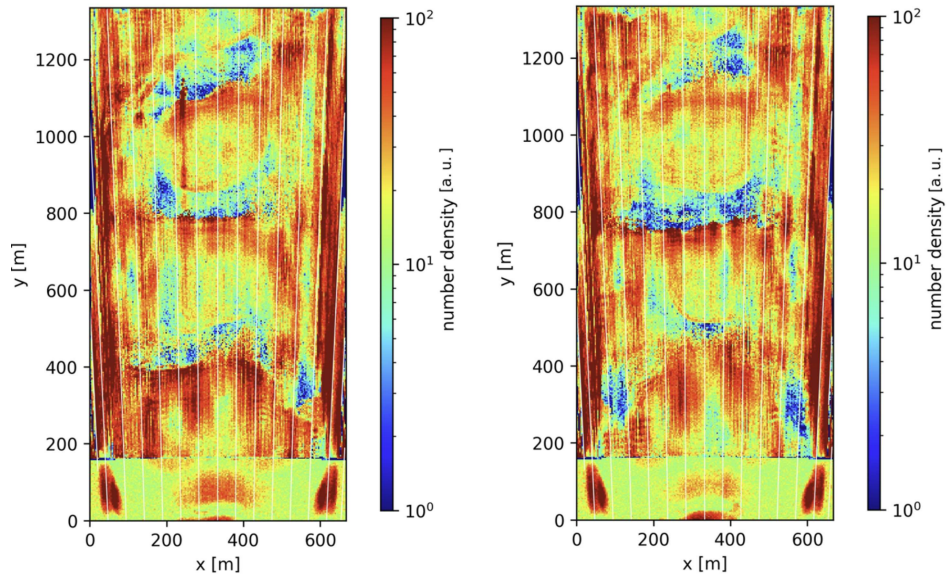

Figure 4.7: Comparison of the total number density at the end of the simulation. They have different values of heat deposition depth, on the left is $L = 3 \times 10^{-3}$ cm and on the right $L = 3 \times 10^{-4}$ cm. The gray lines represent the magnetic field lines.

Based on these three simulation cases, we conclude that moderate variations in surface density and heat deposition depth do not play a decisive role in shaping the thermal response of the polar cap region. Although small differences can emerge over time, the overall thermal behavior remains the same. This relative insensitivity can be attributed to the dominant role of radiative cooling in the thermal balance of the system. As a result, the feedback between heating, particle acceleration, and spark events is more governed by the efficiency of radiative losses than by the exact values of surface density or the depth at which energy is deposited.

4.7 Large-scale simulations

Additionally, I also performed two large-scale simulations to obtain better resolution and to learn to work with a supercomputer. Together with my colleague Bc. Jakub Gazdoš, we applied and gained access to the supercomputer Karolina in the 32nd Open Access Grant Competition by IT4Innovations, with limited computational time.

The initial parameters of the simulations are in Table 4.2. The setup is the same as in the small-scale simulations, but the resolution is higher. With the grid size $\Delta = 83.386$ cm, the real size of the domain is again 667m $\times$ 1334m. The star surface is located around $200\Delta \approx 167$m on the y axis.

Table 4.2: Parameters for large-scale simulations.

Parameter	Value
Star period	0.25 s
Star mass $M_\star$	$1.5\,\mathrm{M}_\odot$
Star radius $R_\star$	10 km
Dipole inclination i	0°
Dipole field B_{dipol}	10^{12} G
Dimensions	$800\Delta \times 1600\Delta \times 1\Delta$
Timestep	$6000\Delta t$
Grid cell size Δ	83.39 cm
Simulation timestep Δt	1.39 ns
Plasma frequency ω_p	$1.6 \times 10^8\,\mathrm{s}^{-1}$
$\omega_\mathrm{p}\Delta t$	0.223
Friedman filter θ	0.1
Particle decay threshold γ_th	5×10^8
Initial surface temperature T_s	10^6 K
Critical ion temperature T_ion	1.01×10^6 K
Depth of heat deposition L	0.003 cm
Surface density ρ_s	$4.45 \times 10^3\,\mathrm{g/cm}^3$
Thermal conductivity of the surface κ	1.6×10^{11} erg/cm/s/K

To compare and find the effects of heating and cooling of the surface, in one simulation, the thermal effects are turned off, and in the second one are turned on. The total number density at the end of the simulation comparison is in Figure 4.8. Small symmetrical bunches are being created in the simulation without the thermal effect. On the other hand, in the simulation with thermal effect, small irregularities in the bunches can be seen. The difference is very small, and a longer simulation is needed to analyze several spark cascades.

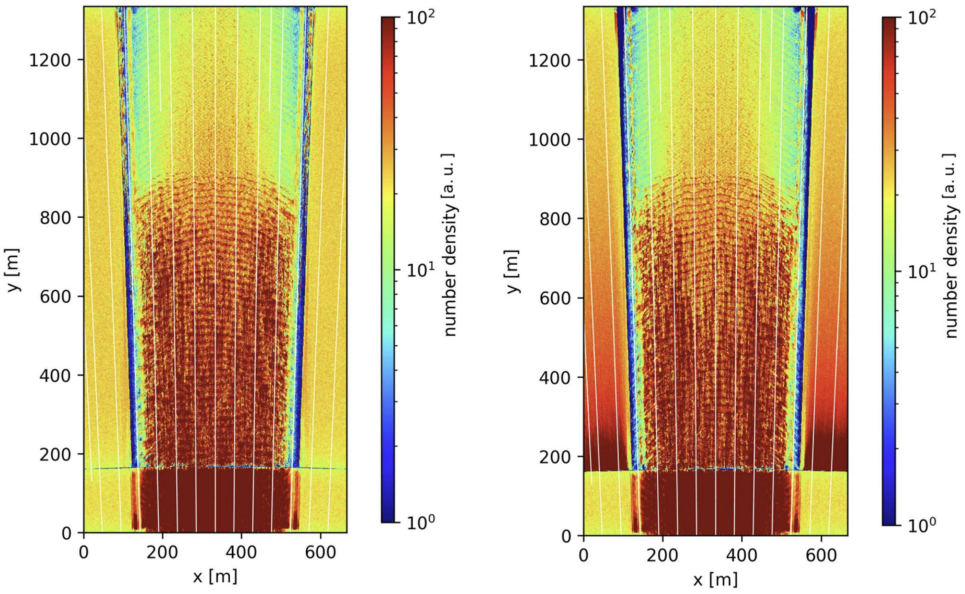

Figure 4.8: Comparison of the total number density in two different large-scale simulations at the end of the simulation. One simulation is without the thermal effects (left) and one with the thermal effects (right). The gray lines represent the magnetic field lines.

Conclusion

The primary goal of this thesis was to develop a new kinetic numerical model that self-consistently describes thermal processes at the neutron star surface and examines their feedback on the cascade in the pulsar polar cap. I performed a series of 2D particle-in-cell (PIC) simulations using the ACRONYM code, allowing for comparison and study of the effects of surface heating and cooling mechanisms on cascade dynamics.

The thesis begins with an overview of the astrophysical context of pulsars, outlining their discovery, key observational features, such as periodic radio emission, strong magnetic fields, and spin-down energy loss, and the theoretical framework of the rotating dipole model. Concepts such as open versus closed magnetic field lines and the Goldreich-Julian charge density are introduced as foundations for understanding pulsar magnetospheres.

The second chapter focuses on the plasma environment near the polar cap, where acceleration gaps and pair cascades originate. Several inner acceleration region (IAR) models are discussed, with special attention given to the partially screened gap (PSG) model. The PSG model provides a physical basis for subpulse drifting and nulling, linking these phenomena to $E \times B$ drift of plasma bunches.

Chapter three introduces numerical methods, particularly the role of PIC simulations in modeling relativistic plasma in pulsar environments. The structure of the ACRONYM PIC code was described along with an implementation of a theoretical thermal model based on Gil et al. (2003), incorporating both heating from returning particles and cooling mechanisms.

In the final chapter, the simulation setup is presented in detail with parameters given in Table 4.1. The equations governing thermal surface evolution are described in Section 4.2, and my contributions to two related publications are summarized in Section 4.1. The performed simulations demonstrate that the temperature stabilizes in response to heating and cooling, validating the implementation. Results show that blackbody radiation dominates over heat transport (see Figure 4.3) in the regulation of the surface temperature. Simulations with different initial parameters reveal that variations in surface density and heat deposition depth have only minor effects on the cascade structure, as shown in Figure 4.6 and 4.7. While heating can raise the surface temperature to the critical point for ion emission, rapid cooling limits the long-term impact on pair production.

Large-scale simulations performed on the Karolina supercomputer confirm the findings of smaller simulations, though further work with greater runtime is necessary to draw stronger conclusions. Overall, the inclusion of thermal feedback into the PIC code definitely affects plasma bunches and

cascade dynamics, though deviations from the theory, such as the absence of clear screening or cascade suppression, indicate that additional or different physical processes may need to be incorporated to fully describe and understand the mechanisms behind pulsar radio emission.

Bibliography

Abbott, B. P., Abbott, R., Abbott, T. D., Acernese, F., Ackley, K., Adams, C., Adams, T., Addesso, P., Adhikari, R. X., Adya, V. B., Affeldt, C., Afrough, M., Agarwal, B., Agathos, M., Agatsuma, K., Aggarwal, N., Aguiar, O. D., Aiello, L., Ain, A., … Chua, S. (2017). GW170817: Observation of Gravitational Waves from a Binary Neutron Star Inspiral., *119*(16), Article 161101, 161101. https://doi.org/10.1103/PhysRevLett.119.161101

Acronym pic code. (n.d.). https://plasma.nerd2nerd.org/

Baade, W., & Zwicky, F. (1934). On super-novae. *Proceedings of the National Academy of Sciences*, *20*(5), 254–259. https://doi.org/10.1073/pnas.20.5.254

Backer, D. C. (1970). Pulsar Nulling Phenomena., *228*(5266), 42–43. https://doi.org/10.1038/228042a0

Basu, R., & Mitra, D. (2018). Subpulse drifting, nulling, and mode changing in PSR J1822-2256., *476*(1), 1345–1355. https://doi.org/10.1093/mnras/sty297

Basu, R., Mitra, D., & Melikidze, G. I. (2017). Meterwavelength single-pulse polarimetric emission survey. iii. the phenomenon of nulling in pulsars. *The Astrophysical Journal*, *846*(2), 109. https://doi.org/10.3847/1538-4357/aa862d

Basu, R., Mitra, D., Melikidze, G. I., & Maciesiak, K. (2025). Pulsar coherent radio emission from solitons : Average emission properties. https://arxiv.org/abs/2504.12163

Basu, R., Mitra, D., Melikidze, G. I., Maciesiak, K., Skrzypczak, A., & Szary, A. (2016). Meterwavelength single-pulse polarimetric emission survey ii. the phenomenon of drifting subpulses. *The Astrophysical Journal*, *833*(1), 29. https://doi.org/10.3847/1538-4357/833/1/29

Benáček, J., Jessner, A., Pohl, M., Rievajová, T., & Oswald, L. S. (submitted in March 2025). On the origin of radio polarization in pulsar polar caps [Preprint]. https://arxiv.org/abs/2503.17249

Benáček, J., Timokhin, A., Muñoz, P. A., Jessner, A., Rievajová, T., Pohl, M., & Büchner, J. (2024). Poynting flux transport channels formed in polar cap regions of neutron star magnetospheres., *691*, Article A137, A137. https://doi.org/10.1051/0004-6361/202450949

Borghese, A., & Zelati, F. C. (2025). The zoo of isolated neutron stars. https://arxiv.org/abs/2502.17652

Crinquand, B., Cerutti, B., Dubus, G., Parfrey, K., & Philippov, A. (2021). Synthetic gamma-ray light curves of Kerr black hole magnetospheric

activity from particle-in-cell simulations., *650*, Article A163, A163. https://doi.org/10.1051/0004-6361/202040158

Cruz, F., Grismayer, T., Torres, R., Chen, A. Y., Spitkovsky, A., Fonseca, R. A., & Silva, L. O. (2024). Particle-in-cell simulations of pulsar magnetospheres: Transition between electrosphere and force-free regimes., *690*, Article A229, A229. https://doi.org/10.1051/0004-6361/202347926

Cruz, F., Grismayer, T., Chen, A. Y., Spitkovsky, A., & Silva, L. O. (2021). Coherent emission from qed cascades in pulsar polar caps. *The Astrophysical Journal Letters*, *919*(1), L4. https://doi.org/10.3847/2041-8213/ac2157

Drake, F. D., & Craft, H. D. (1968). Second Periodic Pulsation in Pulsars., *220*(5164), 231–235. https://doi.org/10.1038/220231a0

Esirkepov, T. Z. (2001). Exact charge conservation scheme for Particle-in-Cell simulation with an arbitrary form-factor. *Computer Physics Communications*, *135*(2), 144–153. https://doi.org/10.1016/S0010-4655(00)00228-9

Esirkepov, T. Z. (1999). Exact charge conservation scheme for particle-in-cell simulations for a big class of form-factors. https://arxiv.org/abs/physics/9901047

Friedman, A. (1990). A second-order implicit particle mover with adjustable damping. *Journal of Computational Physics*, *90*(2), 292–312. https://doi.org/https://doi.org/10.1016/0021-9991(90)90168-Z

Gajjar, V., Joshi, B. C., Kramer, M., Karuppusamy, R., & Smits, R. (2014). Frequency independent quenching of pulsed emission. *The Astrophysical Journal*, *797*(1), 18. https://doi.org/10.1088/0004-637x/797/1/18

Gil, J., Lyubarsky, Y., & Melikidze, G. I. (2004). Curvature Radiation in Pulsar Magnetospheric Plasma., *600*(2), 872–882. https://doi.org/10.1086/379972

Gil, J., Melikidze, G. I., & Geppert, U. (2003). Drifting subpulses and inner acceleration regions in radio pulsars*. *AA*, *407*(1), 315–324. https://doi.org/10.1051/0004-6361:20030854

Goldreich, P., & Julian, W. H. (1969). Pulsar Electrodynamics., *157*, 869. https://doi.org/10.1086/150119

Greenwood, A. D., Cartwright, K. L., Luginsland, J. W., & Baca, E. A. (2004). On the elimination of numerical Cerenkov radiation in PIC simulations. *Journal of Computational Physics*, *201*(2), 665–684. https://doi.org/10.1016/j.jcp.2004.06.021

Harding, A. K. (2001, April). Gamma-ray pulsars: Models and predictions. In F. A. Aharonian & H. J. Völk (Eds.), *High energy gamma-ray astronomy: International symposium* (pp. 115–126, Vol. 558). AIP. https://doi.org/10.1063/1.1370785

Harding, A. K., & Muslimov, A. G. (1998). Particle Acceleration Zones above Pulsar Polar Caps: Electron and Positron Pair Formation Fronts., *508*(1), 328–346. https://doi.org/10.1086/306394

Herfindal, J. L., & Rankin, J. M. (2007). Periodic nulls in the pulsar B1133+16., *380*(2), 430–436. https://doi.org/10.1111/j.1365-2966.2007.12089.x

Herfindal, J. L., & Rankin, J. M. (2009). Deep analyses of nulling in Arecibo pulsars reveal further periodic behaviour., *393*(4), 1391–1402. https://doi.org/10.1111/j.1365-2966.2008.14119.x

Hessels, J. W. T., Ransom, S. M., Stairs, I. H., Freire, P. C. C., Kaspi, V. M., & Camilo, F. (2006). A Radio Pulsar Spinning at 716 Hz. *American Astronomical Society Meeting Abstracts #207*, *207*, Article 209.07, 209.07.

Hewish, A., Bell, S. J., Pilkington, J. D. H., Scott, P. F., & Collins, R. A. (1968). Observation of a Rapidly Pulsating Radio Source., *217*(5130), 709–713. https://doi.org/10.1038/217709a0

Kelner, S. R., Prosekin, A. Y., & Aharonian, F. A. (2015). Synchro-curvature radiation of charged particles in the strong curved magnetic fields. *The Astronomical Journal*, *149*(1), 33. https://doi.org/10.1088/0004-6256/149/1/33

Kilian, P., Burkart, T., & Spanier, F. (2012). The Influence of the Mass Ratio on Particle Acceleration by the Filamentation Instability. *High Performance Computing in Science and Engineering '11*, 5–13. https://doi.org/10.1007/978-3-642-23869-7_1

Konar, S., & Deka, U. (2019). Radio pulsar sub-populations (i): The curious case of nulling pulsars. *Journal of Astrophysics and Astronomy*, *40*(5). https://doi.org/10.1007/s12036-019-9608-z

Labaj, M., Benáček, J., & Karlický, M. (2024). Particle-in-cell simulations of electron-positron cyclotron maser forming pulsar radio zebras., *681*, Article A113, A113. https://doi.org/10.1051/0004-6361/202346600

Longair, M. S. (2011). *High Energy Astrophysics*. Cambridge University Press.

Lorimer, D. R., & Kramer, M. (2004). *Handbook of Pulsar Astronomy* (Vol. 4). Cambridge University Press.

Lyne, A., & Graham-Smith, F. (2012). *Pulsar astronomy* (4th ed.). Cambridge University Press.

Lyutikov, M. (2013). Inverse compton model of pulsar high-energy emission. *Monthly Notices of the Royal Astronomical Society*, *431*(3), 2580–2589. https://doi.org/10.1093/mnras/stt351

Lyutikov, M., Otte, N., & McCann, A. (2012). The very high energy emission from pulsars: A case for inverse compton scattering. *The Astrophysical Journal*, *754*(1), 33. https://doi.org/10.1088/0004-637x/754/1/33

Manthei, A. C., Benáček, J., Muñoz, P. A., & Büchner, J. (2021). Refining pulsar radio emission due to streaming instabilities: Linear theory and pic

simulations in a wide parameter range. *Astronomy amp; Astrophysics*, *649*, A145. https://doi.org/10.1051/0004-6361/202039907

McSweeney, S. J., Bhat, N. D. R., Wright, G., Tremblay, S. E., & Kudale, S. (2019). The frequency-dependent behavior of subpulse drifting. i. carousel geometry and emission heights of psr b0031–07. *The Astrophysical Journal*, *883*(1), 28. https://doi.org/10.3847/1538-4357/ab3a97

Melikidze, G. I., Gil, J. A., & Pataraya, A. D. (2000). The spark-associated soliton model for pulsar radio emission. *The Astrophysical Journal*, *544*(2), 1081–1096. https://doi.org/10.1086/317220

Mitra, D., Melikidze, G., & Gil, J. (2015). Coherent radio emission from pulsars. https://arxiv.org/abs/1510.00103

Oppenheimer, J. R., & Volkoff, G. M. (1939). On Massive Neutron Cores. *Physical Review*, *55*(4), 374–381. https://doi.org/10.1103/PhysRev.55.374

Pacini, F. (1967). Energy Emission from a Neutron Star., *216*(5115), 567–568. https://doi.org/10.1038/216567a0

Philippov, A., Timokhin, A., & Spitkovsky, A. (2020). Origin of pulsar radio emission. *Phys. Rev. Lett.*, *124*, 245101. https://doi.org/10.1103/PhysRevLett.124.245101

Philippov, A. A., Spitkovsky, A., & Cerutti, B. (2015). Ab initio pulsar magnetosphere: Three-dimensional particle-in-cell simulations of oblique pulsars. *The Astrophysical Journal*, *801*(1), L19. https://doi.org/10.1088/2041-8205/801/1/l19

Rengarajan, T. N. (1973). Radio Emission from Pulsars and Surface Temperature of Neutron Stars. *Nature Physical Science*, *242*(120), 102–104. https://doi.org/10.1038/physci242102a0

Rievajová, T. (2023). *Particle-in-cell simulations of sparking event in pulsar polar caps* [Bachelor's Thesis]. Masaryk university, Brno. https://is.muni.cz/auth/th/ac4al/

Ritchings, R. T. (1976). Pulsar single pulse intensity measurements and pulse nulling., *176*, 249–263. https://doi.org/10.1093/mnras/176.2.249

Rosswog, S., & Brüggen, M. (2007). *Introduction to High-Energy Astrophysics*. Cambridge University Press.

Ruderman, M. A., & Sutherland, P. G. (1975). Theory of pulsars: polar gaps, sparks, and coherent microwave radiation., *196*, 51–72. https://doi.org/10.1086/153393

Soudais, A., Cerutti, B., & Contopoulos, I. (2024). Scaling up global kinetic models of pulsar magnetospheres using a hybrid force-free-pic numerical approach. *AA*, *690*, A170. https://doi.org/10.1051/0004-6361/202450238

Szary, A., Melikidze, G. I., & Gil, J. (2015). Two modes of partially screened gap., *447*(3), 2295–2306. https://doi.org/10.1093/mnras/stu2622

Timokhin, A. N., & Harding, A. K. (2019). On the maximum pair multiplicity of pulsar cascades. *The Astrophysical Journal*, *871*(1), 12. https://doi.org/10.3847/1538-4357/aaf050

Vay, J.-L., Geddes, C., Cormier-Michel, E., & Grote, D. (2011). Numerical methods for instability mitigation in the modeling of laser wakefield accelerators in a lorentz-boosted frame. *Journal of Computational Physics*, *230*(15), 5908–5929. https://doi.org/https://doi.org/10.1016/j.jcp.2011.04.003

Wang, N., Manchester, R. N., & Johnston, S. (2007). Pulsar nulling and mode changing. *Monthly Notices of the Royal Astronomical Society*, *377*(3), 1383–1392. https://doi.org/10.1111/j.1365-2966.2007.11703.x

Weltevrede, P., Edwards, R. T., & Stappers, B. W. (2006). Statistics of the drifting subpulse phenomenon. https://arxiv.org/abs/astro-ph/0605201

Weltevrede, P. (2016). Investigation of the bi-drifting subpulses of radio pulsar b183904 utilising the open-source data-analysis project psrsalsa. *AA*, *590*, A109. https://doi.org/10.1051/0004-6361/201527950

Wen, Z. G., Wang, N., Yuan, J. P., Yan, W. M., Manchester, R. N., Yuen, R., & Gajjar, V. (2016). Investigation of nulling and subpulse drifting properties of PSR J1727-2739., *592*, Article A127, A127. https://doi.org/10.1051/0004-6361/201628214

Xu, Y. H., Wen, Z. G., Yuan, J. P., Wang, Z., Duan, X. F., Wang, Z., Wang, N., Wang, M., Wang, H. G., Rusul, A., Hao, L. F., & Han, W. (2024). Investigation of individual pulse emission behaviors from pulsar j1741–0840. *The Astrophysical Journal*, *977*(1), 90. https://doi.org/10.3847/1538-4357/ad7fe2